First International Conference on
Bio-based Building Materials

June 22nd - 24th 2015
Clermont-Ferrand, France

PERMEABILITY AND THERMAL CONDUCTIVITY OF PRE-CAST LIME AND HEMP CONCRETE

V. Picandet*[1], P. Tronet[1], T. Colinart[1], T. Lecompte[1], M. Choinska[2]

[1] Université de Bretagne Sud, Laboratoire d'Ingénierie des Matériaux de Bretagne,56100 Lorient
[2] L'Université Nantes Angers Le Mans, GéM, IUT de Saint-Nazaire, 44600 Saint-Nazaire

*Corresponding author; vincent.picandet@univ-ubs.fr

Abstract
Lime and Hemp Concrete (LHC), used as building material, shows a wide range of densities and mix proportions and, as a consequence, various mechanical and thermal properties. The hemp shiv used as aggregate in such concrete is highly porous, with a low specific apparent density and a low thermal conductivity compared to the binder matrix. Shiv in bulk can be compressed to reduce significantly its volume since shiv particles are highly deformable. As a consequence, for same mix proportioning by weight, various densities can be achieved, depending on the casting process and the compaction applied on the fresh mix. This paper focuses on pre-cast elements made of compacted LHC. The fresh mixes are cast in a compression die with a controlled load. The binder and water contents are lower than conventional mixes cast in site. The pre-cast process has been accurately defined to achieve high reproducibility of blocks even if a slight density gradient occurs into the specimens due to wall friction during compaction. This process leads to lower void ratio into the LHC. The mechanical resistance is significantly improved while the increase in thermal conductivity is minor since the weight proportion of binder paste is lower. The ability of hemp concrete to regulate the indoor relative humidity is well known, and sometime not perfectly explained. The air permeability of such material gives a first indicator about the water vapor transfer ability of the LHC but any study has focused on its measurement. Our experiments show the changes in permeability and thermal conductivity induced by the compaction relative to this casting process for various mix designs.

Keywords: Permeability, Thermal conductivity, Durability, Mass transfers, Shiv

1 INTRODUCTION

Density and mix design of lime and hemp concrete (LHC) are key parameters to control the mechanical behavior as well as the thermal conductivity of the in-service material. As shown in many previous studies, the mechanical performance of such composite can be drastically changed when the mass content of bio-based granular increases [Nguyen 09] [Nguyen 10], [Tronet 14b].

Globally, the mechanical resistance tends to increase when the density of the hardened material increases, but mix proportion has also a great influence on the mechanical behavior. For instance, previous studies demonstrate that a part of the mass amount of binder paste could advantageously be substituted by hemp shiv [Nguyen 10]. Hence, for equivalent density, higher bearing capacities are achieved while lower increase in thermal conductivity is observed when the shiv content (in kg/m^3 of LHC) increases.

Moreover, reduction of binder content is beneficial since the hydraulic, aerial limes and other pozzolanic materials have the greater environmental foot print among the constituents used in such building material.

However, increase in shiv content required compaction to cast the LHC blocks. Experience show that in site manual casting limits the shiv content to a maximum about 200 kg/m^3. Higher shiv content can only be achieved using a compacting device. Currently, devices able to induce a stress of 8 to 10 MPa on the fresh mix have been investigated [Nguyen 09] [Tronet 14b].

Manual casting or spraying process usually needs high water to binder ratio that could be detrimental for the mechanical resistance of the hardened binder paste. Compacting process does not need any workability of the concrete since the mix can be poured in the mould as it is, even with a dry appearance. Actually, reduction of the binder content induces reduction in the water content. As a consequence, the water is mainly or completely absorbed by the uncompacted shiv when the water is added to the mix before pouring in the mould, i.e. the compacting die. Compaction will wring the shiv to release enough water to ensure the hydration of the

binder at the end of the process. Such process allows accurate setting of the water amount according to binder need.

Casting by compaction induces preferential orientation of shiv particles that are usually elongated due to the porous structure of the woody core of the stem [Picandet 13]. Pouring of the pulverulent or dry-like mix into the die induces almost any significant preferential orientation, except those due to the wall effect. Compaction will reduce the volume according to only one direction and induces as a consequence a preferential orientation of the particles according to the orthogonal plan of the compaction axis. Anisotropic thermal and mechanical properties of such compacted concrete have been already studied [Nguyen 09] [Nguyen 10] [Tronet 14b]. Indeed, to get more benefit of such induced anisotropic properties into the material, pre-cast elements have to be well positioned into the walls to get the better building performance.

This study focuses on the permeability of such compacted LHC and explores the limit of highly compacted concrete. The permeability is only measured according to the compaction directions. In case of anisotropic permeability, the lowest permeability is theoretically obtained according to this axial direction.

The mix designs studied are first presented and some observations of their porous structure through microtomograhy and SEM are commented. The gas permeability tests are then introduced to explain the specific experimental protocol applied to such permeable "concrete". The permeability results are finally discussed according to the mix parameters but also according to many other measurement such as applied stress upon the fresh mix during compaction or water loss of the sample that corroborate ability of water vapor to migrate through the material during the curing stage.

Finally, thermal conductivity measurements according to axial and radial directions are presented to complete a set of data needed to discuss the limit in building application of such highly compacted concrete. Lower permeability lets suppose lower rate of water vapor transfer and possible condensation effect, altering thermal resistance and durability of the wall.

2 MIX DESIGN AND CASTING PROCESS

2.1 Aggregates

In this study, the shiv has been totally separated from fibers using a mechanical grinding process. This bio-based aggregate is characterized by a very low bulk density (about 110 kg/m^3) because of its highly porous structure. As a consequence, this aggregate exhibits a high water absorption capacity, up to 270% after a few minutes [Nguyen 09] [Chamoin 11]. Particle density of shiv is 280 kg/m^3 measured by Pham [Pham 14].

2.2 Binder

A lime based binder called Tradical ® PF 70 (Lhoist group) was used. It consists in 75% hydrated lime $Ca(OH)_2$, 15% hydraulic lime, and 10% pozzolana. Its specific density, given by the supplier, is 2450 kg/m^3.

2.3 Mix design

Based on Nguyen thesis [Nguyen 10], five LHC mixes were designed to explore the suitability of mixtures with a high shiv proportion (i.e. low binder proportion), by applying quite high pressures in a cylindrical matrix. The capillary and deformable character of shiv makes mixing process different than for traditional concrete or mortars which behave as a soft material with consistency of paste. The mixing phase consists in two steps: 1–Mixing of shiv and water during 4 minutes at 140 rpm in a planetary Hobart mixer; 2– Adding lime and mixing during 4 minutes at 140 rpm. In the first step, the water is totally absorbed by the shiv. This means that the second step is similar to a mixing of solid particles. Water is released by aggregates as they are pressed in the compression die. The amount of water needs to be calculated as a function of binder content, considering that shiv remain water saturated at the end of compaction process and the excess water released is available for the binder hydration.

The mix contents are presented in Tab. 1 where compactness designates the volume fraction that is filled. W/B is the Water to Binder mass ratio, equal to 0.55 for each LHC mixture. B/S is the Binder to Shiv mass ratio. The shiv mass is based on dry shiv, i.e. oven-dried at 60°C until to a constant weight (for two or three days in ventilated oven).

Tab 1. Mix designs in kg/m^3 of LHCs studied

	M1	**M2**	**M3**	**M4**	**M5**
Shiv (**S**)	215	257	320	500	500
Binder (**B**)	388	360	320	271	204
Water (**W**)	213	198	176	149	112
B/S ratio	1.8	1.4	1	0.54	0.41
W/B ratio	0.55	0.55	0.55	0.55	0.55
Green Density	816	816	816	920	816
Green Compactness	0.52	0.52	0.52	0.6	0.52
Hardened Compactness	0.38	0.41	0.43	0.56	0.51

The compression device is composed of a steel 100 mm-inner-diameter cylinder, a fixed lower punch, and a moving upper punch, see Figure 1. The piston rod of the upper punch is screwed under a 250 kN press, equipped with force and displacement transducers. The thickness of the cylinder wall is 10 mm, ensuring a negligible strain up to a radial pressure of 10 MPa. More details are available in [Tronet 14a].

The initial (bulk) apparent volume of the mixture poured into the cylinder is three to four times the final compacted apparent volume. The target value for the final height is 20 cm for each specimen. The casting process is controlled in displacement, with the same upper punch speed of 1 mm/s. Fig. 2 shows the compacted sample after it is pulled out of the matrix.

The mean upper pressure σ_{zUP} can be deduced from the force transducer measurement F_{UP} of the press:

$$\sigma_{zUP} = F_{UP} / \pi R^2 \quad (1)$$

where *R* is the inner radius of the compression die (see Fig. 1).

At the end of the compression step, the specimen reaches a given compactness, called "green compactness" reported in Tab. 1. Compactness is the most significant parameter to characterize the compaction state, due to the difference of specific gravity between water, shiv and lime. At fresh state, compactness corresponds to the sum of solid volume fraction and liquid volume fraction, i.e. the ratio of liquid and solid volumes by total volume of the sample. The liquid phase is included because it is assumed to be physically linked to lime and shiv at the end of compression step without volume decrease due to initiation of lime hydration and chemical shrinkage. This assumption is also valid as soon as the water content is low, ensuring that no free and draining water exits from the sample. The mixes studied are designed to ensure any loss of mass is due to excess of water at the end of the compaction. Weight measurements of the compacted specimens check this assumption.

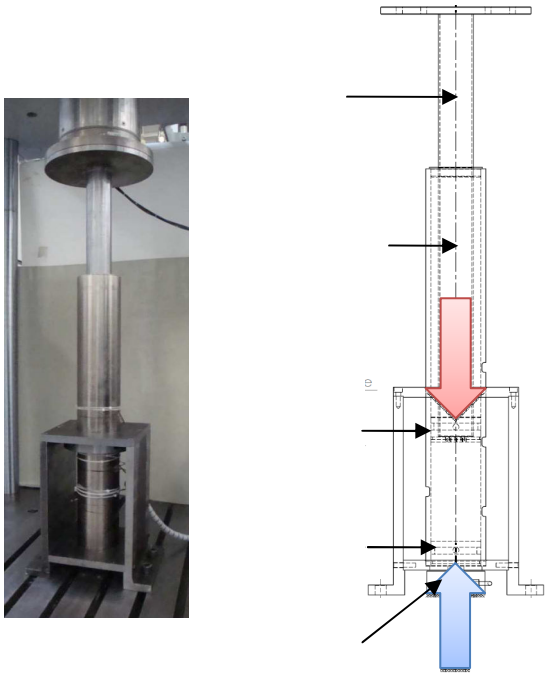

Fig. 1: Compression device used for casting [Tronet 14a] [Tronet 14b].

At the end of compression process, each specimen is maintained in compression, keeping a height of 200 mm, during 72 hours. This step is needed to ensure a minimum hydration of lime, avoiding capping and elastic release of the specimen when pushing out of the die. LHC cylindrical specimens as shown in Fig. 2 are then placed in a room controlled in temperature (20±1°C) and relative humidity (70±5%), until the age of 90 days. The most compacted specimens (M4 and M5) must also be clamped during maturation to avoid any visco-elastic release.

Fig. 2: Compacted specimen after casting [Tronet 14a].

It should be noted that mixes M1, M2, M3 and M5 have been designed to target the same green compactness at the end of the compaction while M4 is an intermediate mix designed to add more binder into the mix M5 to bridge the Binder to shiv ratio (B/S) between M3 and M5 (see Tab. 1). It is supposed to provide more mechanical resistance than M5. M4 as M5 is the mix with the highest shiv content, but M4 is designed to avoid the need of clamping after few days curing.

During ageing of LHC specimens, some liquid water is consumed by lime hydration and a large amount is evaporated. Then the compactness of samples decreases, as shown in Tab. 1. Globally, it should be noted that final compactness decreases when paste or water content increases.

3 MICROSTRUCTURE CONSIDERATION

3.1 Hemp shiv characteristics

Shiv comes from the plant stem. Its porous structures and global shape is strongly oriented according to the stem axis [Picandet 13]. As a consequence, the hemp straw process leads to elongated and flaky particles with various contents of cortical fibers remaining, see Fig. 3. In this study, the selected hemp shiv comes from a complete un-fibering process and contains less than 2 % of short bast fibers by weight [Nguyen 09].

a) b)

Fig. 3: Picture of bulk hemp shiv a) and of cross section of hardened M1 LHC specimen b).

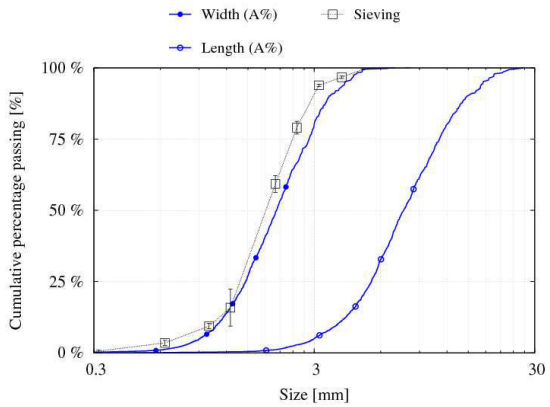

Fig. 4: Size distribution of shiv particles based on cumulative mass obtained by mechanical sieving and size- distribution based on cumulative projected area obtained by image analysis.

Granular packing in concrete strongly depends on Particle Size Distribution (PSD), even with highly deformable granular. To minimize the inter-granular porosity, well graded or wide regular PSD is generally required. In case of LHC, granular has high volume content, and may also be preferentially oriented due to casting process. The mechanical, thermal and transfer properties of LHC should then strongly depend on the PSD of shiv particles, and on the particle shape as well. Fig. 4 shows the cumulative distribution obtained with mechanical sieving and image analysis based on 2D observation of flaky particles. According to the projected area of the particles, uni-modal distributions of both particle width and length are generally observed with shiv particles [Picandet 13]. Median length about 8 mm and median width about 2 mm has been observed with respectively 1.6 and 1.7 mm standard mean deviations as indicator of the particle sorting. The elongation ratio of particles is about 4 and remains the same whatever the considered size range of the distribution with a significant standard deviation about 2mm, indicating large varieties of aspects and shapes. Experimental protocol and analysis are detailed in [Picandet 13].

3.2 Specimen heterogeneity

Casting process using compaction does not produce blocks with perfect homogeneity. Due to friction along the inner form wall, the compression stress decreases in the lower part of the die. The force measured at the bottom of the die (see Fig. 1) is always lower than the applied upper force, F_{UP}. As a consequence, a slight decrease of the density is observed in lowest section of the specimens [Nguyen 09]. To control the quality of the blocks and identify its main cause, the friction is measured using specifically-designed instrumented die [Tronet 14a].

In this study, the selected mix designs induce only limited heterogeneities inside compacted blocks. However, in order to evaluate the incidence of the cast-induced heterogeneity on compactness and permeability, three 50 mm thick discs are extracted from each specimen as shown in Fig. 5. The mean density or compactness of the discs theoretically slightly decreases from the top to the bottom.

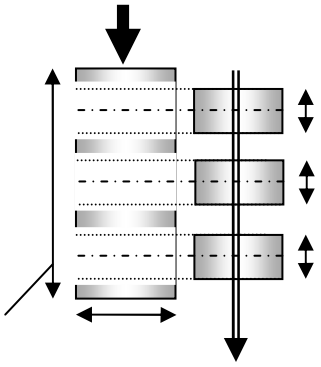

Fig. 5: Extraction of the discs for the permeability test.

3.3 Anisotropy

In the present case, anisotropy is most of all induced by the shiv particles, which are elongated and flaky. As soon as the mixture is poured in the die, particles tend already to lie on their widest surface to form successive layers. But the significant strain applied to material by the compacting process induces the most significant preferential orientation of the shiv particles according to the cross section plan, i.e. the plan perpendicular to the load direction. The observation of vertical sections of specimens shown in Fig. 6 confirms this preferential horizontal orientation.

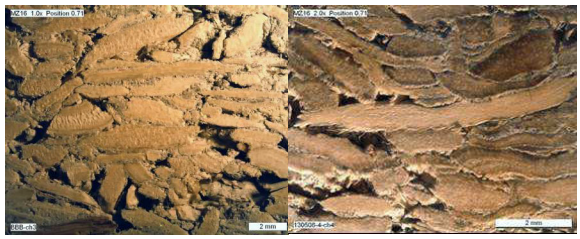

a) b)

Fig. 6: Observation of preferential orientation of hemp shiv particles from vertical (axial) section of compacted material with a upper stress lower than 0,5 MPa a) and more than 1 MPa b).

Microtomography gives a 3D analysis of the orientation of the particles and of the microstructure of the compacted LHC. In this study, one prismatic sample has been extracted from each middle disc, as shown in Fig. 7, in order to correlate observations with the permeability measurements of the middle disc.

Analysis of the core samples confirms the decrease in inter-granular porosity and the significant orientation of the micro structure inside compacted LHC. The Fig. 8 shows picture of a vertical (axial) section of the specimens the less and the most compacted specimen (M1 and M5 respectively) at mid height.

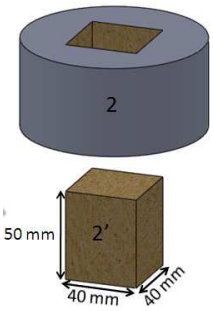

Fig. 7: Extraction of a prismatic sample from the permeability tested middle height discs [Tronet 14b]

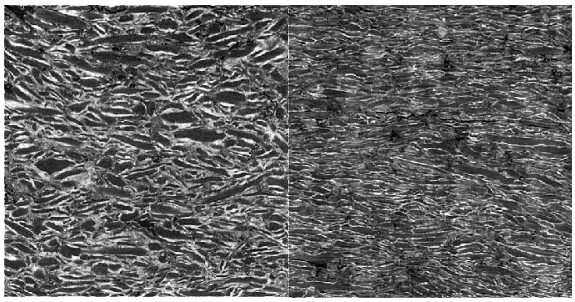

a) Mix M1 b) Mix M5

Fig. 8: Microtomography of vertical (axial) section of specimen M1 a) and M5 b) showing the anisotropy inside compacted material and preferential orientation of the shiv particles inside specimens [Tronet 14b].

Inside granular, the porosity is also significantly anisotropic since the cell wall are strongly oriented according to the stem axis, see Fig. 9. The average capillaries length is about 80 µm while their diameters range from 10 to 50 µm in uncompacted shiv particles [Nguyen 09]. This orientation coincides with the major axis length of aggregates [Picandet 13] to produce a multi-scale anisotropy from inter to intra-granular porosity.

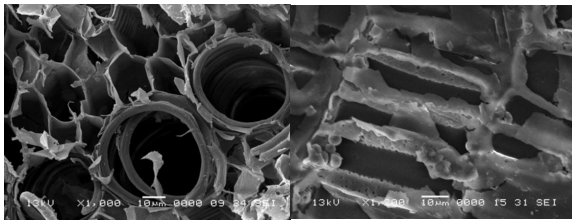

a) b)

Fig. 9: Scanning Electron Microscope (SEM) pictures with different magnifications of longitudinal section a) and cross section c) of hemp shiv particle b) of a hemp shiv particle [Nguyen 09].

4 PERMEABILITY MEASUREMENTS

4.1 Sample preparation

The tested samples are the discs extracted from the cast cylindrical specimen (see Fig. 5). Gas permeability depends on the saturation degree of the porous structure. Discs are dried at 60°C in ventilated oven until constant weight, generally for 2-3 weeks, in order to consider gas-saturated permeability measurements.

4.2 Gas permeability device

The permeability measurements are carried out in an air-conditioned room regulated at (20 ± 1°C) using a constant head permeameter, known as Cembureau permeameter, and nitrogen as neutral percolation fluid. A general layout of the device designed to measure gas permeability of concrete [Kameche 14], is given in Fig. 10. Each disc is subjected to a constant inlet pressure P_i at the lower surface while the outlet pressure is the atmospheric pressure, P_{atm} (see Fig. 10). After initiating the percolation, sufficient time (few minutes) is needed for the establishment of steady-state flow before measurement. The pressures, as well as the flow rates, are recorded during the tests. Both inlet and outlet gas flow rates are measured using thermal mass flow meters of different capacities in order to check if any gas leakage occurs. For each differential pressure, the apparent coefficient of permeability k_A (m²) is calculated from the Hagen-Poiseuille relationship considering laminar and isothermal flow of a compressible viscous fluid through a porous body, using the following well-known relationship:

$$k_A = \frac{Q}{A}\frac{2\mu\, LP_{atm}}{(P_i^2 - P_{atm}^2)} \quad (2)$$

where L is the thickness of the sample (m), A is the cross-sectional area (m²), Q is the measured gas flow at atmospheric pressure (m^3/s), μ is the coefficient of viscosity ($1{,}76.10^{-5}$ Pa.s for N_2 gas at 20°C), P_i is the inlet pressure. Each disc is tested at five differential pressures, P_i, ranging from 4 to 20 kPa.

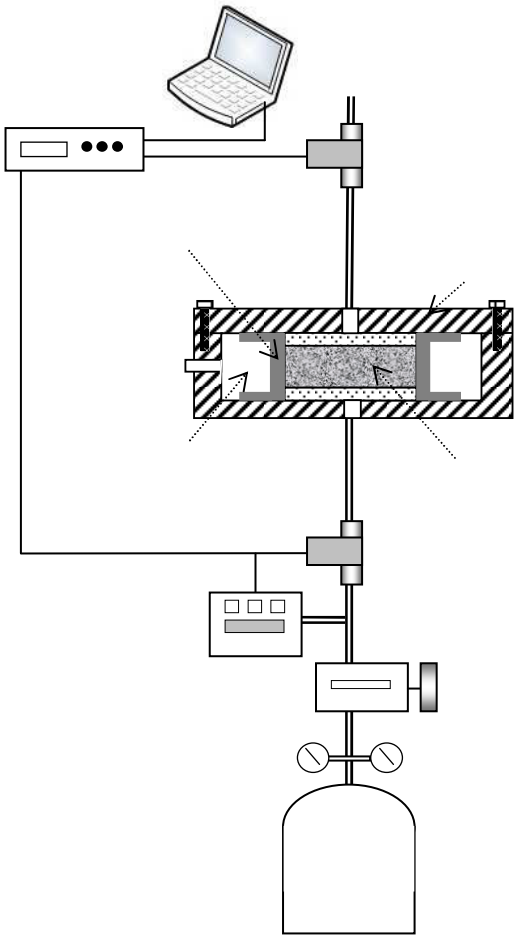

Fig. 10: Experimental gas permeability set-up

k_A usually depends on the applied mean pressure, $P_{meam} = (P_i + P_{atm})/2$, due to slip (or Knudsen) flow whether to inertial (or turbulent) flow that takes place in the global gas flow trough samples [Picandet 09]. The LHC permeability ranges from 5.10^{-13} to 10^{-12} m^2. It is high compared to those of usual hydraulic concrete, about $10^{-16}m^2$. As a consequence, the slight decrease in the apparent permeability with increasing gradient pressure is mainly due to inertial flow that could be deduced using the Dupuit-Forcheimer's law.

$$\frac{1}{k_A} = \frac{1}{k_V} + B_t \frac{Q}{A} \quad (3)$$

where k_v is the intrinsic permeability, relative to the pure viscous flow, and B_t is a constant parameter deduced from several measurements for various flow rates, i.e. for various inlet pressures [Picandet 09]. Thereafter only intrinsic permeability value, k_v, is considered. It is deduced from five measurements at least of apparent permeability k_A, obtained with various inlet pressures. Error estimations are based on standard deviation beside the mean values obtained according the extrapolation law in eq. (3).

4.3 Effect of upper compaction load and compactness on permeability of specimens

As expected, higher compacting stresses increase compactness of specimens and reduce the pore volume inside material. As a consequence, the mean radius of the percolating path becomes narrow and the global permeability decreases. In Fig. 11, an exponential regression fit well the relationship between applied upper stress, σ_{zUP} defined in eq.(1), and the decrease in axial permeability for the mixes except M4 having a higher green compactness.

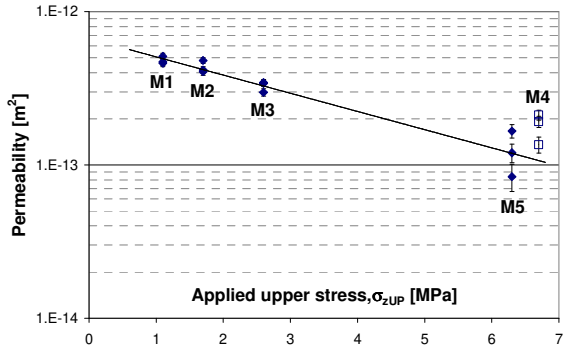

Fig. 11: Axial intrinsic gas permeability of compacted LHC according to applied compacted stress, σ_{zUP}.

The final compactness of discs is obtained after a complete drying at 60°C (see § 4.1). Fig. 12 shows a global exponential correlation between compactness and decrease in permeability of LHC, but it should be noted that M4 with higher binder content than M5 (see § 2.3) departs again.

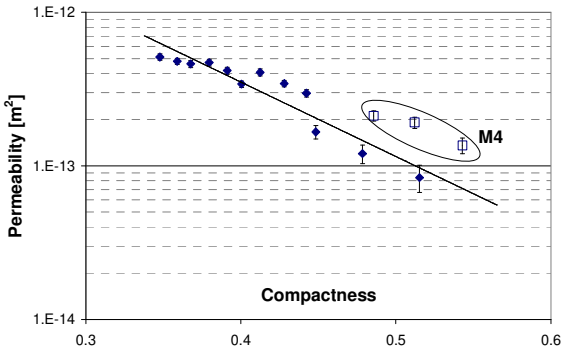

Fig. 12: Axial intrinsic gas permeability of compacted LHC according to final compactness.

4.4 Effect of permeability on moisture loss after curing and drying

The first effect of permeability on specimens can be observed after the curing stage, i.e. after 90 days at 70 ± 5% HR. A linear relationship appears in Fig. 13 between the water loss inside specimens and its mean permeability. This point corroborates the link between the permeability of the specimens and their ability to transfer moisture.

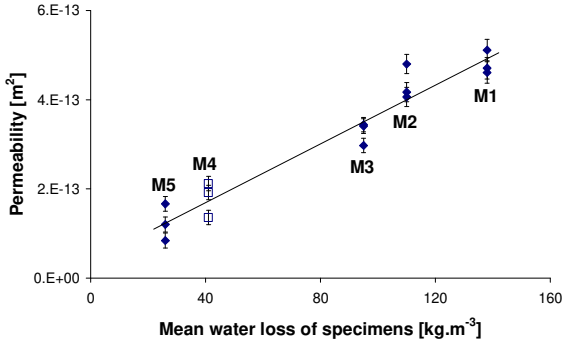

Fig. 13: Axial intrinsic gas permeability of compacted LHC according to mean moisture loss after curing.

The decrease in permeability toward the bottom of the specimen, where the compacting stress and the final compactness is lower, explains the spreading of the results for a given specimen and its mean water loss.

After a drying at 60°C until constant weight, a linear relationship between permeability and water loss is also observed in Fig. 14, but only for specimen having the same green compactness (i.e. except M4).

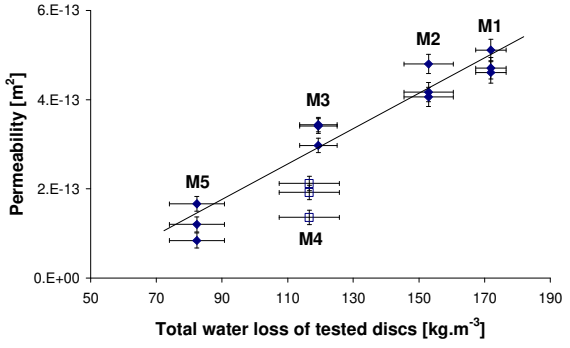

Fig. 14: Axial intrinsic gas permeability of compacted LHC according to mean water loss after drying.

Comparison between M4 and M5 shows that higher binder paste content tends to increase significantly the water loss of specimens. Even with an initial low water to binder ratio (i.e. W/B = 0.55), water remains in excess at the end of the curing stage. This let suppose a significant porosity inside the hardened binder paste.

4.5 Effect of binder paste volume fraction on permeability

The binder paste volume fraction inside specimen, in m^3 per m^3 of LHC, is here considered as an apparent volume without any shrinkage effect due to hydration. The Fig. 15 clearly shows that permeability tends to increase exponentially with the mean binder paste volume fraction inside specimen.

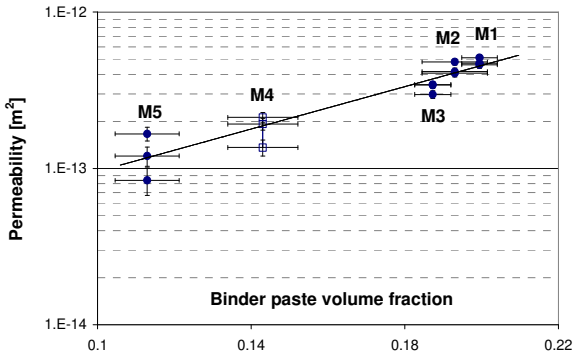

Fig. 15: Axial intrinsic gas permeability of compacted LHC according to binder paste volume fraction.

This result lets suppose that binder paste has higher permeability than granular, i.e. compacted shiv particles. Higher content of binder paste would create more inter-granular porosity by reducing rearrangement of particles at the beginning of the compacting process.

4.6 Effect of shiv content on permeability

For a same green compactness to target, the casting upper stress mainly depends on the shiv content [Tronet 14]. In such a case, a noticeable exponential correlation appears between shiv content and permeability of each disc, see Fig. 16. Shiv content is here deduced from the density of each disc assuming that mix proportion remains constant wherever inside the specimen.

With similar compaction process, many authors have already observed such kind of relationship between the density of wood or kenaf fiber network and its permeability [Imtiaz 14]. The following empirical relationship has been proposed [Thoemen 08]:

$$k_v = \exp\left(a + b\rho + c/\ln(\rho)\right) \quad (4)$$

where *a*, *b* and *c* are the constant parameters of the model and ρ is the fiber density corresponding here to the shiv content inside the LHC in kg/m^3.

Generally, the value of last parameter *c* deduced after fitting of the experimental results is very low [Thoemen 08]. The fitting of our results, neglecting *c*, tends to define *a* = -27.1 and *b* = -5.2 10^{-3}.

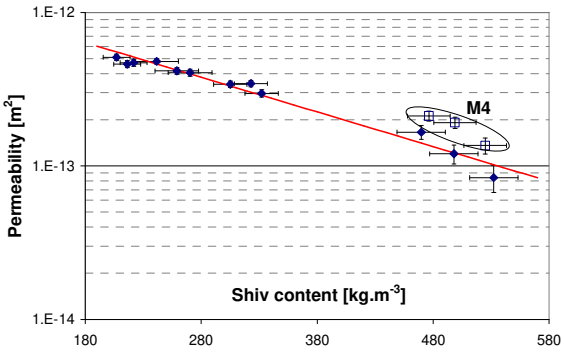

Fig. 16: Axial intrinsic gas permeability of compacted LHC according to deduced shiv content into samples.

It should be noted that results from the mix M4 have not been considered to establish this correlation since the green density departs from the other. As already shown in § 4.5, compared to the mix M5, the higher content of binder paste increases the permeability of the hardened mix M4 despite higher green compactness and applied stress for casting.

It is worth to note that resin impregnation used to bind such bio-based fibers induces a slight decrease in permeability of compacted material [Imtiaz 14]. Unlike organic binder, lime-based binder seems to increases the permeability of the compacted material when binder content increases.

5 THERMAL CONDUCTIVITY

5.1 Sample preparation

Beside the effect of particles orientation induced by the casting process, the capillary structure of the shiv, i.e. the woody core part of the stem (see Fig. 9), results also in anisotropic thermal properties of compacted LHC [Nguyen 09]. For instance, the longitudinal thermal conductivity inside wood (parallel to the capillaries in the stem axis) is higher than the cross one [Carré 90]. As shown in Fig. 6, the macroscopic thermal conductivity should be then higher in horizontal (or radial) direction than in vertical (or axial) direction inside specimens. 60 mm x 60 mm x 30 mm prismatic samples are extracted from the cast cylindrical specimens at different heights. 3 are cut according to the vertical plan and 4 are cut according to horizontal plan, see Fig. 17 and Fig. 19.

Samples are dried at 60°C in ventilated oven until constant weight, for seven days at least, prior testing.

5.2 Experimental set up

The thermal conductivity of material is measured at a mean temperature close to 20°C, using a stationary heat flow method, known as guarded hot plate. The device used was developed in the laboratory and already described in previous studies, see [Nguyen 09]. The measurement uncertainties (±0.5 mm in sample thicknesses, ±1mm in lateral dimensions, ±0.5°C in temperature measurements and ±0.2 mW in dissipated or inlet power) lead to a thermal conductivity uncertainty about 7% [Carré 1990].

5.3 Horizontal or radial thermal conductivity

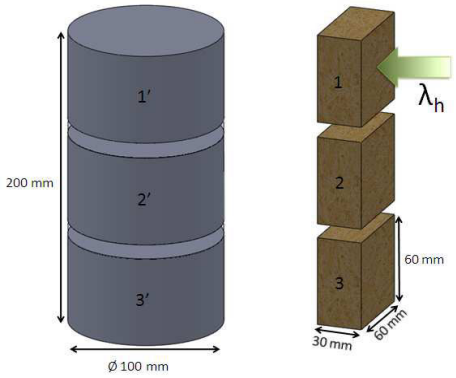

Fig. 17: 3 samples for thermal conductivity measurement according to the horizontal (or radial) direction are extraxted from cast specimens.

The thermal conductivity globally increases with dried compactness (or density) of the specimens. Uncertainty relative to its measurement is also plotted as abscise error bars in Fig. 18 and Fig. 20.

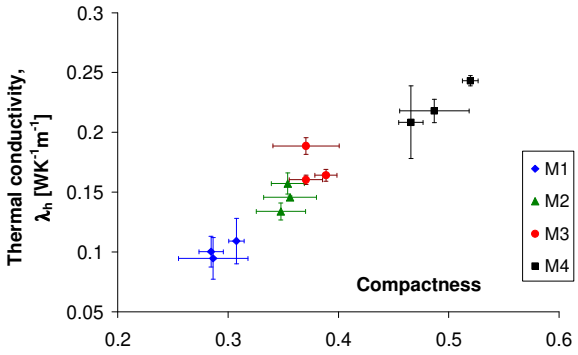

Fig. 18: Horizontal (or radial) thermal conductivity versus compactness of dried samples.

As shown in Fig. 18, the horizontal thermal conductivity increases almost linearly with the compactness of the material. The conductivity of the oriented shiv with their oriented cell walls made of lignin and interfaces made of hardened binder paste would constitute the main thermal conductors. Increase in the volume fraction of these constituents would lead to this linear effect.

5.4 Vertical or axial thermal conductivity

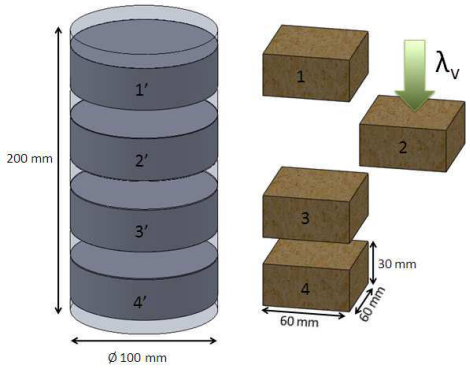

Fig. 19: 4 samples for thermal conductivity measurement according to the vertical (or axial) direction are extracted from cast specimens

The air voids would constitute the main thermal insulators in such configuration. According to the general rule of mixture, this thermal conductivity is theoretically the closest of the Reuss or lower bound. In such a case, the preferential orientation of the porous structure is the main regulator of the heat flux. In this configuration, unlike permeability, thermal conductivity does not increase significantly when compactness increases, as shown in Fig. 20, since higher compaction would magnify the preferential orientation of the porous structure in the radial plan and the anisotropy of the densified LHC as shown in Fig. 8.

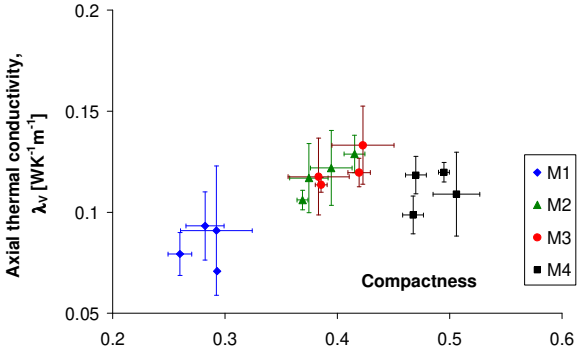

Fig. 20: Vertical (or axial) thermal conductivity versus compactness of dried samples.

6 CONCLUSION

In this study, for the first time to our knowledge, gas permeability of densified LHC has been investigated, in correlation with thermal conductivity measurements. Permeability of the studied LHCs are lower than 4 orders of magnitude compared to manually cast LHCs but remain higher than cellular concrete [Cerezo 2005].

Only the axial permeability, parallel to the compacting load of LHC has been investigated. Due to anisotropic properties of LHC, the lower permeability and thermal conductivity are observed in this axial direction, that is, representative for instance of mass transfers through pre-cast compacted LHC panels used as insulation layer in building construction. The radial permeability is assumed to be higher, but with values of the same order. From this assumption, many incidences on the in-service materials can be deduced.

The benefits of compacting process on mechanical properties of LHC have been already studied [Nguyen 09], [Tronet 14b] and its consequence on some transfer properties are here mainly studied through comparisons between the mixes M1, M2, M3 and M5. Hence, the increase in substitution of binder paste with hemp shiv in LHC leads to:

- Higher compaction stress on the fresh LHC mix to cast for a given green compactness (i.e. density just after casting).
- Decrease in axial permeability. As a consequence, in-service compactness increases significantly since water loss is significant in such concrete, even with low initial water to binder ratio (W/B = 0.55).
- No significant increase in axial (or vertical) thermal conductivity, while, as expected, almost linear increase of the radial (or horizontal) one.

Finally, comparison of M4 and M5 gives unexpected results: increase in binder paste content for given shiv content tends to increase the LHC permeability.

This would mean that hardened binder paste is more permeable inside specimen than the compacted hemp shiv.

Mass transfer inside LHC strongly depends on the hardened binder paste needing further investigations. Finally, the ability of in-service LHC to avoid water condensation and molds issues should be considered also as a durability criterion needing finest evaluations.

7 ACKNOWLEDGMENTS

This research was partly supported by environmental research initiative of “Fondation de France” and European Community through a state/region contract plan (FEDER).

8 REFERENCES

[Carré 90] Carré P, Le Gall R, “Définition et détermination des conductivités thermiques dans la structures multicouches C.V.R. – balsa”, Revue générale de thermique, 1990, 340.

[Cerezo 05] Cerezo V. Propriétés mécaniques, thermiques et acoustiques d’un matériau à base de particules végétales: approche expérimentale et modélisation théorique. PhD thesis, Ecole Nationale des travaux publics de l’état, 2005.

[Chamoin 11] Chamoin J, Collet F, Pretot S, Lanos C. Réduction du pouvoir absorbant de chènevottes par traitement imperméabilisant, Matériaux & Techniques 2011, EDP Sciences, 99(6), 633–641.

[Imtiaz 14] Imtiaz A., Krishnan J., Debes B. Implications of fiber characteristics and mat densification on permeability, compaction and properties of kenaf fiber panels, Ind. Crops and Prod. 2014, 61:293–302

[Kameche 14] Kameche Z.A, Ghomari F, Choinska M, Khelidj A, Assessment of liquid water and gas permeabilities of partially saturated ordinary concrete, Construction and Building Materials 2014, 65:551–565

[Nguyen 09] Nguyen TT, Picandet V, Carré P, Lecompte T, Amziane S, Baley C. Effect of compaction on mechanical and thermal properties of hemp concrete, European Journal of Environment and Civil Engineering 2009,13:1039–1050.

[Nguyen 10] Nguyen TT. Contribution à l’étude de la formulation et du procédé de fabrication d’éléments de construction en béton de chanvre, PhD thesis, Université de Bretagne-Sud, 2010.

[Pham 14] Pham TH, Modélisation multi-échelles des propriétés thermiques et élastiques de composites chaux-chanvre, PhD thesis, Université de Bretagne-Sud, 2014.

[Picandet 09] Picandet V, Khelidj A, Bellegou H, Crack effects on gas and water permeability of concretes, Cem Concr Res 2009,39:537–547

[Picandet 13] Picandet V, Characterization of Plant-Based Aggregates. In: Amziane S, Arnaud L, editors. Bio-aggregate-based Building Materials. London/Hoboken: ISTE/Wiley, 2013:27-73.

[Thoemen 08] Thoemen H, Walther T, Wiegmann A, 3D simulation of macroscopic heat and mass transfer properties from the microstructure of wood fibre networks, Composites Science and Technology 2008, 68:608–616

[Tronet 14a] Tronet P, Lecompte T, Picandet V, Baley C. Study of lime and Hemp composite precasting by compaction of fresh mix – A Fitted die to measure friction and stress state, Powder Technology, 2014, 258:285–296.

[Tronet 14b] Tronet P, contribution à l’étude des matériaux chaux-chanvre: influence du compactage sur les propriétés, PhD thesis, Université de Bretagne-Sud, 2010.